Flow Science Report 08-15

Development of the Compliant Mooring Line Model for *FLOW-3D*®

Gengsheng Wei
Flow Science, Inc.
October 2015

---

1. Introduction

Mooring systems are common in offshore structures, ship mooring and renewable energy harvesters. The existing springs-and-ropes model in ***FLOW-3D*** allows multiple elastic ropes to be tethered to moving objects. The main assumption of the model is that the rope's mass can be ignored. This assumption translates into the following simplifications:

- The ropes are weightless.
- The ropes are always straight in shape when they are in tension.
- Rope tension is uniform along the rope and is simply proportional to the rope's extension and the spring constant.

These simplifications limit the applications of the elastic ropes to mooring systems. Although the elastic rope model may work for light, taut mooring lines, it is invalid for catenary or heavy mooring lines where the mooring line weight cannot be neglected compared to the tension forces. Because rope dynamics is not considered, the model cannot accurately determine the tension force of a mooring line on a structure and thus cannot accurately calculate the structure motion. In addition, it is unable to calculate the tension distribution, maximum tension and the shape of the mooring lines.

To overcome these limitations, a compliant mooring line model has been developed and implemented in ***FLOW-3D***® version 11.1. Using a finite segment approach, the model numerically calculates the full 3D dynamics of the mooring lines and the dynamic coupling between the mooring lines and tethered moving objects. Multiple mooring lines with different lengths, diameters, mass densities and other physical properties are allowed to exist in one simulation. A mooring line can have both of its ends connected to moving objects or one end connected to a moving object and the other anchored at a fixed location. Mooring lines can be taut or slack and may fully or partially rest on the sea/river bed. Gravity, buoyancy, fluid drag and tension are considered for calculations of motion and instantaneous shape of the mooring lines. Static equilibrium is assumed for the initial condition of each line.

The model allows the mooring lines to be partially or completely outside the computational domain. When a line is anchored deep in the water, depending on the vertical size of the domain, the lower part of the line can be located outside the domain, where there is no computation of fluid flow. In this case, it is assumed that a uniform

water current exists below the domain for that part of the mooring line, and the corresponding drag force is evaluated based on the uniform deep-water velocity.

Model limitations exist, off course. Bending stiffness and interaction between mooring lines are not considered. When simulating mooring line networks, free nodes are not allowed. Collisions with solid objects are also not considered, thus overlap between mooring lines and objects could occur.

2. Theory and Method

The model uses a finite segment approach to calculate the 3D dynamics of mooring lines with the assumption that the mooring lines are compliant cylinders with uniform diameter and material distribution. As shown in Figure 1, a mooring line is divided uniformly into N discrete segments. Let L_0 denote the undisturbed length of the mooring line; the undisturbed length of a segment is then $l = L_0/N$. Each of the segments is represented by a mass point located at the segment center with three degrees of freedom. The equation of motion for the mass point is

$$m_p \frac{d\vec{v}_p}{dt} = \vec{G} + \vec{B} + \vec{T}_1 + \vec{T}_2 + \vec{D}_n + \vec{D}_t \quad (1)$$

On the left-hand side, m_p is mass of the segment, and $\vec{v}_p$ is the mass point velocity. The terms on the right-hand side represent forces that are shown in Figure 2. $\vec{G}$ is the gravitational force; $\vec{B}$ is the buoyancy force calculated using Archimedes' principle; $\vec{T}_1$ and $\vec{T}_2$ are the tension forces between the mass particle and the neighbor particles at its two sides; $\vec{D}_n$ and $\vec{D}_t$ are the fluid drag forces in normal and tangential directions of the segment. $\vec{B}$, $\vec{D}_n$ and $\vec{D}_t$ are considered only for mass points that are submerged in water.

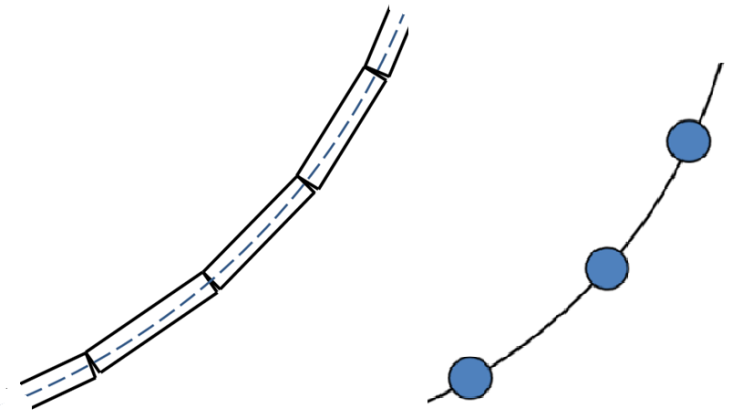

Figure 1. Discrete segments of a mooring line and the mass point representation of the segments.

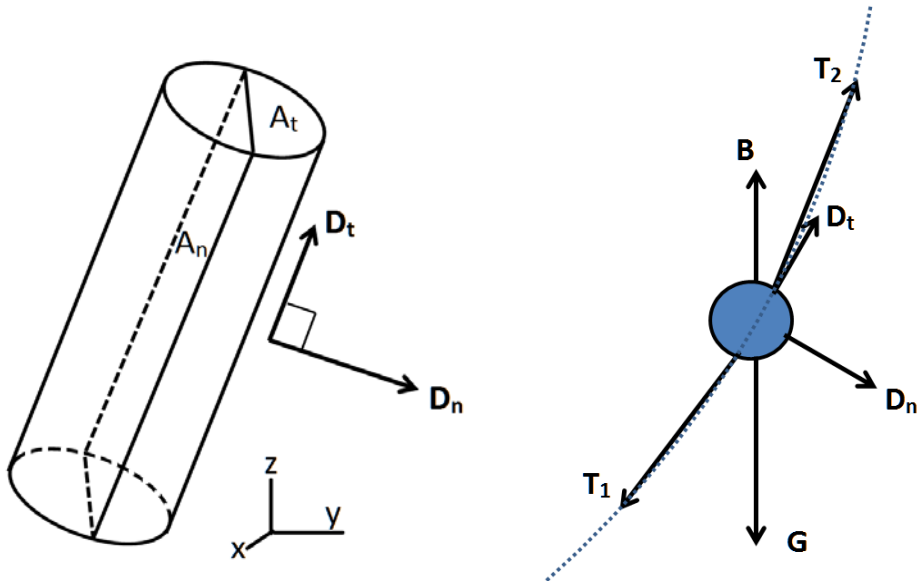

Figure 2. Forces applied to a mooring line segment at its mass point.

$\vec{T}_1$ and $\vec{T}_2$ are calculated using the Hooke's law

$$\vec{T}_1 = k_l \Delta l_1, \quad \vec{T}_2 = k_l \Delta l_2 \tag{2}$$

where Δl_1 and Δl_2 are extensions of the mooring line between the mass particle and its two immediate neighbors; k_l is the spring coefficient of a mooring line segment,

$$k_l = k_{unit}/L_0 \tag{3}$$

k_{unit} is spring coefficient per unit length of the undisturbed mooring line. If its value is not available, it can be estimated using the Young's modulus of the material, *E*, and the net cross-sectional area of the mooring line, A_{net}, as follows

$$k_{unit} = EA_{net} \tag{4}$$

$\vec{D}_n$ and $\vec{D}_t$ in Equation (1) are evaluated using the quadratic drag law

$$\vec{D}_n = -C_{D,n}\rho_f A_n \vec{v}_{r,n}|\vec{v}_r| \tag{5}$$

$$\vec{D}_t = -C_{D,t}\rho_f A_t \vec{v}_{r,t}|\vec{v}_r| \tag{6}$$

where $C_{D,n}$ and $C_{D,t}$ are the drag coefficients in the normal and the tangential directions of the segment, respectively; $\vec{v}_r$ is the velocity of the mass particle relative to fluid flow

$$\vec{v}_r = \vec{v}_p - \vec{v}_f \tag{7}$$

where $\vec{v}_f$ is fluid velocity; $\vec{v}_{r,n}$ and $\vec{v}_{r,t}$ are the components of $\vec{v}_r$ in the normal and the tangential directions of the segment, respectively; A_n and A_t are the cross-sectional areas in the normal and tangential directions of the segment, respectively; ρ_f is the fluid density.

At each time step of fluid flow calculation, Equation (1) is solved explicitly for $\vec{v}_p$ of each mass point using a sub-time step numerical algorithm: the main time step is divided into a certain number of sub-time steps to integrate the equation to ensure numerical stability. The sub-time step must be smaller than the time for a longitudinal vibrational wave moving between two neighbor mass points. Location of the mass point is calculated by integrating $\vec{v}_p$ over the sub-time steps. The instantaneous mooring line shape is determined by the updated locations of all the mass points at the end of the integration.

For initial condition, all the mooring lines are assumed to be in static equilibrium. The initial shape of a mooring line is calculated by numerically solving Equation (1) until a steady state is achieved. The first guess of the initial shape of a mooring line is a straight line between its two end points. All the mooring line segments are then released from their first-guessed locations and quickly reach steady state using a high artificial linear damping force that replaces the quadratic damping force defined in Equations (5) and (6). The linear damping force on a mass point follows the equation

$$\vec{D} = -c_l \vec{v}_r \tag{8}$$

Here c_l is the linear damping coefficient, and its value is selected to make the damping ratio η satisfy

$$\eta \equiv \frac{c_l}{2\sqrt{m_p k_l}} > 1.0 \tag{9}$$

Equation (8) means over-damping of the oscillation of the mooring line segments.

When a mooring line is anchored deep in water, the lower part of the line can be located below the computational domain's bottom boundary, where there is no fluid flow computation. In such a case, uniform and constant water velocity $\vec{v}_f$ is assumed for that part of the mooring line, and $\vec{D}_n$ and $\vec{D}_t$ are still evaluated using (5), (6) and (7).

Mooring lines can be restrained in space by upper and lower x, y and z limits if they are defined. For example, a low *z* limit can be used to define a seabed, in which case a mooring line cannot exist below the limit, but can lie partially or completely on the seabed. The tension, extension and horizontal motion are still calculated by solving equation (1) for the part of the mooring line that lies on the seabed.

The dynamic coupling between the mooring lines and the tethered moving objects is implemented by a data exchange between the moving object and mooring line solutions. The moving objects provide the instantaneous locations of the tether ends of the mooring

lines. The mooring line model, in return, supplies tension forces acting on the moving objects at those points.

3. Model Validation and Applications

1) Mooring line in equilibrium

As shown in Figure 3, a compliant catenary cable in equilibrium is suspended between points O and P. The *x* and *z* coordinate axes are set up in horizontal and vertical directions, respectively, with their origins at O. The arc length of the cable from O is *s*. At P, the tension forces in horizontal and vertical directions are F_x and F_z, respectively. Below is the analytical solution originally obtained by Irvin (1981) and later rewritten by Raman-Nair and Baddour (2002). It was used as a benchmark for model validation in DuBuque (2011) and Nichol (2014).

$$x(s) = \frac{F_x s}{k_{unit}} + \frac{F_x}{\rho_l g}\left[\sinh^{-1}\left(\frac{F_z - \rho_l g L_0 + \rho_l g s}{F_x}\right) - \sinh^{-1}\left(\frac{F_z - \rho_l g L_0}{F_x}\right)\right]$$

$$z(s) = \frac{s}{k_{unit}}\left(F_z - \rho_l g L_0 + \frac{1}{2}\rho_l g s\right) + \frac{F_x}{\rho_l g}\left[\sqrt{1 + \left(\frac{F_z - \rho_l g L_0 + \rho_l g s}{F_x}\right)^2} - \sqrt{1 + \left(\frac{F_z - \rho_l g L_0}{F_x}\right)^2}\right]$$

where ρ_l is linear density (mass per unit length) of the cable; g is magnitude of the gravitational acceleration; L_0, again, is the undisturbed cable length.

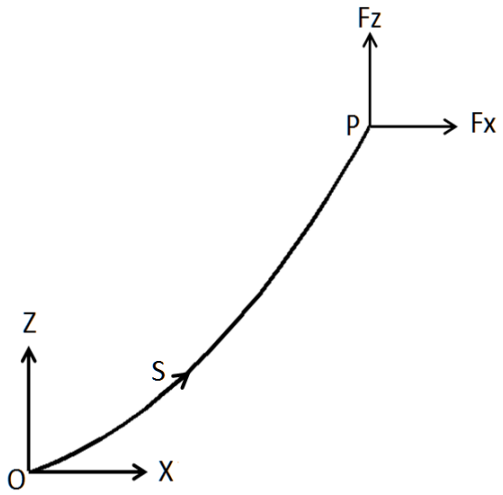

Figure 3. Coordinate system and forces for the elastic catenary.

To compare with the analytical solution, a numerical simulation was conducted using the mooring line model. The cable is assumed to be made from high modulus polyethylene (HMPE) material. Its diameter and undisturbed length are 0.05 m and 100 m,

respectively. Its linear density is 1.904 kg/m, and the spring constant per unit length is 2.095×10^8 N. The cable is suspended between two fixed points with 68 m distance in both horizontal and vertical directions. A total of 30 segments are used to divide the cable. In Figure 4, the cable shape calculated by the mooring line model is compared with that obtained from the analytical solution. The two results match each other very well.

Simulations were also conducted for cables with undisturbed length of 95 m, 100 m and 110 m, and other parameters unchanged. The cable shapes are presented in Figure 5. The cable is taut when L_0 is 95 m and is catenary when L_0 is 100 m or 110 m. For undisturbed length of 110 m, the mooring line is partially suspended, with the rest lying on ground.

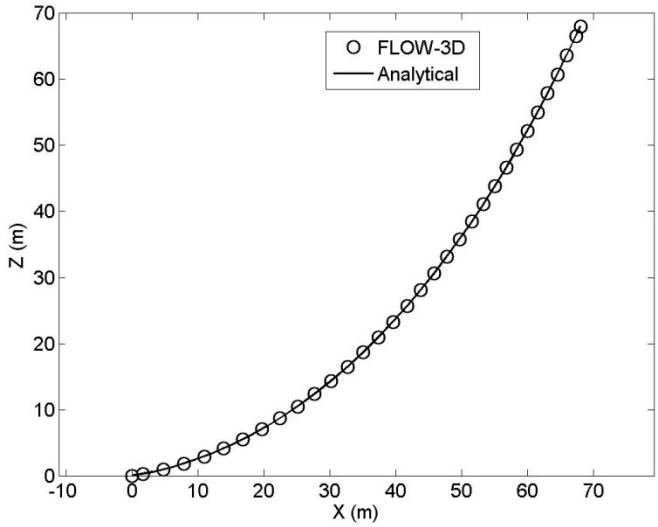

Figure 4. ***FLOW-3D*** result and analytical solution for an elastic catenary.

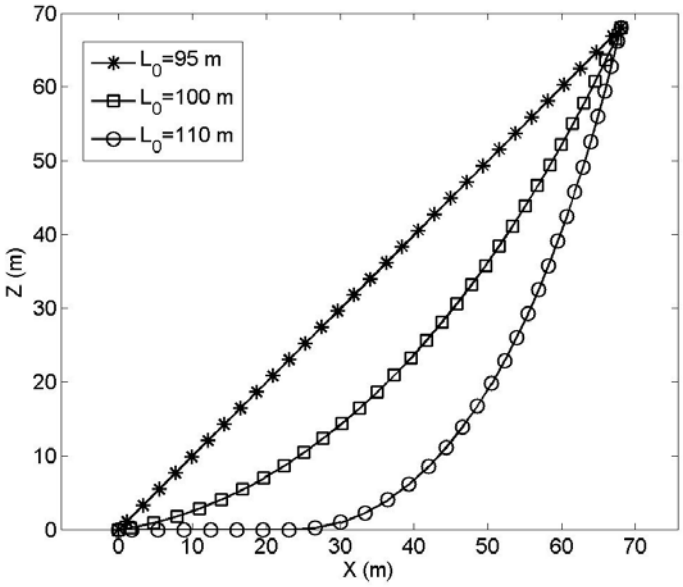

Figure 5. Equilibrium shapes of cables of different length using ***FLOW-3D***.

2) Mooring Lines for a Floating Platform

A simulation was conducted for the interaction of a moored platform with a nonlinear wave in the open sea. The platform deck size is 78 m × 77 m, as shown in Figure 6. The total height of the platform is 105 m. The platform is tethered with twelve mooring lines that are 485 m in length and 0.1 m in diameter. Linear density of the mooring lines is 5.1 kg/m, and the spring coefficient per unit length is 3.7×10^8 N. The nonlinear wave is 10 m in height, with the period of 8 s and wavelength of 100 m, propagating in the $+x$ direction. The water depth is 500 m. The computational domain is 420 m long (in x), 200 m wide (in y) and 130 m deep (in z). To save computational resources, only 50 m of the water depth is included in the computational domain. A rigid, free-slip boundary condition is used at the domain's bottom boundary. This is a reasonable simplification since the wave motion is negligible at the depth equal to half the wavelength according to wave theory (Dean and Dalrymple, 1991). A 100 m long sponge layer is placed immediately before the downstream open boundary where a radiation (outflow) boundary condition is used. The damping coefficient increases linearly from 0 to 1.0 s^{-1} in the sponge layer in the +x direction. Simulation time is 180 s.

The result is shown in Figure 7. The mooring lines are initially in static equilibrium. Driven by the wave, the platform moves and draws the mooring lines in the direction of the wave propagation. Figure 8 shows the x and z coordinates of the platform's mass center versus time. At the end of the simulation, the average position of the platform is maintained in the horizontal direction under the tension force of the mooring lines. In the vertical direction, the platform fluctuates throughout the simulation as the result of the periodic vertical motion of the water surface. The platform position drops vertically over time due to its translation in the x direction and the increased downward pull from the mooring lines as a result.

Figure 9 shows the time-variation of the extension for a line at the front of the platform and another line at the back. Figure 10 presents the maximum tension force of the two mooring lines versus time. Fluctuations are found for both quantities due to the oscillation of the platform with each passing wave. The mooring lines can reach 7.0 m extension and 5.5×10^6 N maximum tension force if they are not broken.

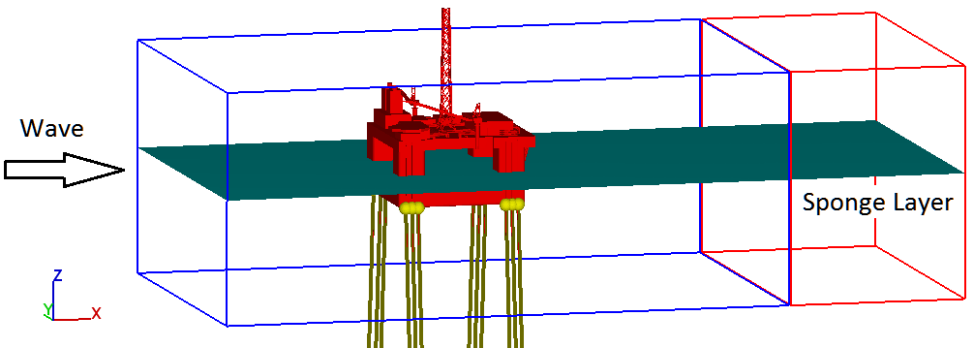

Figure 6. The computational domain and the sponge layer placement.

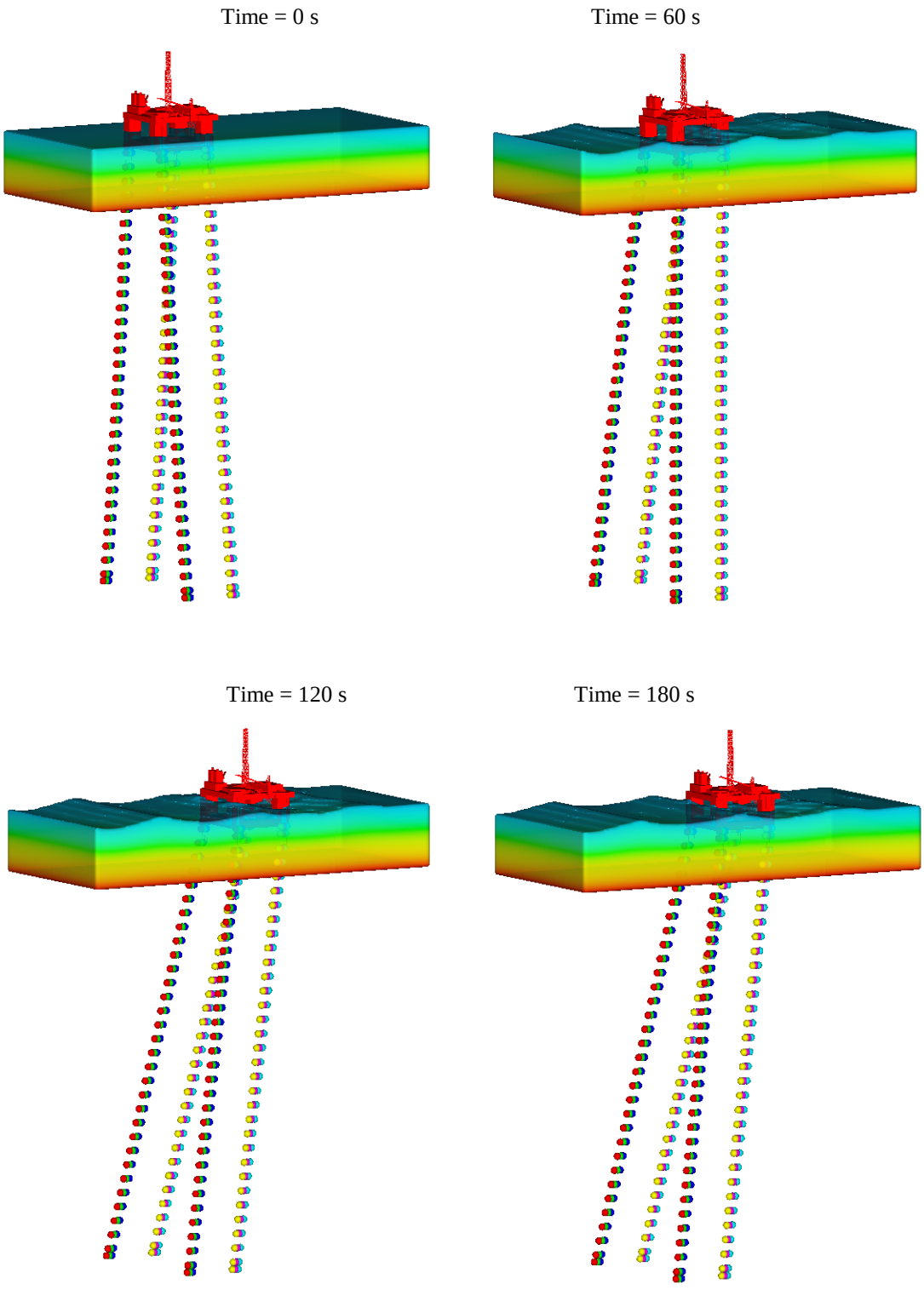

Figure 7. The platform and the wave motion at four different times. The mooring lines are shown as strings of dots. Color represents pressure in the water.

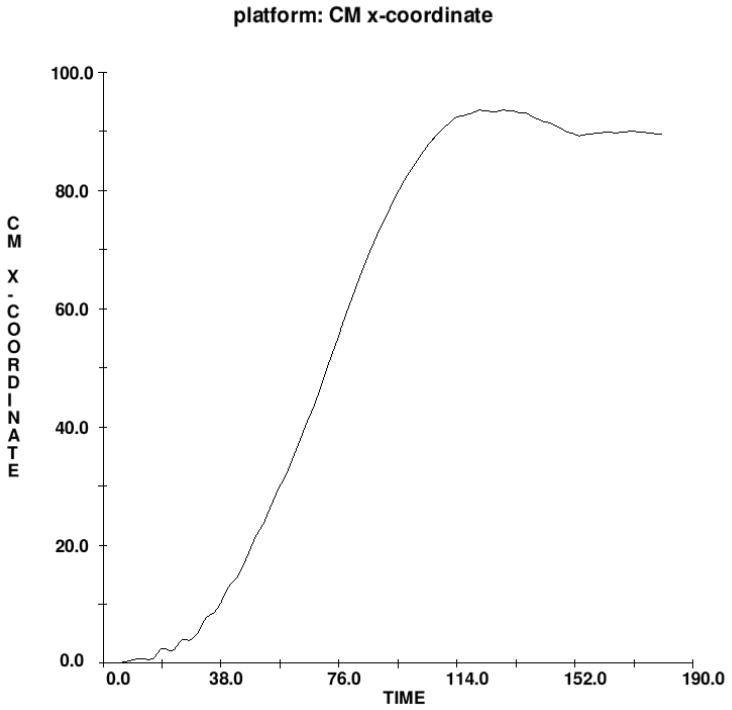

(a)

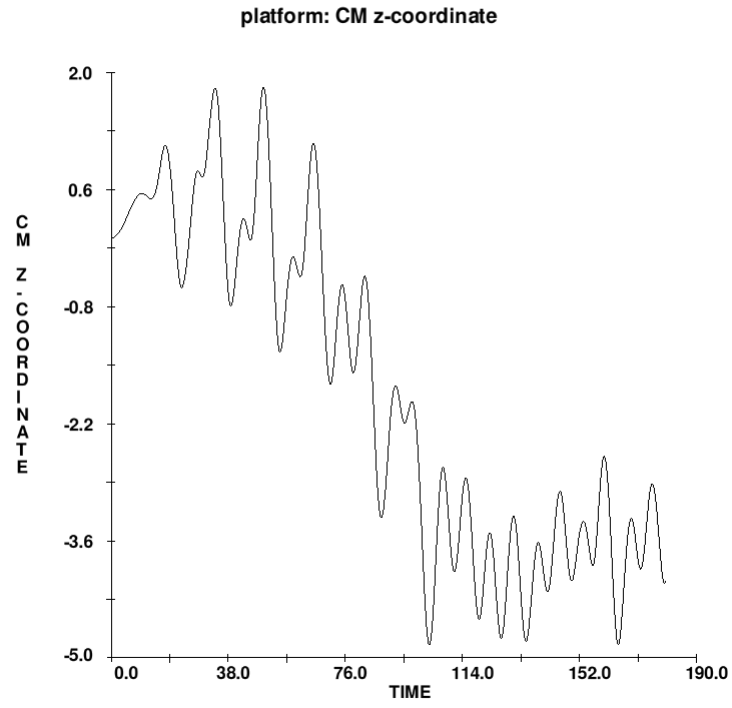

(b)

Figure 8. The *x* and *z*-coordinates of platform mass center (in m) versus time (in s). (a) *x*-coordinate, (b) *z*-coordinate.

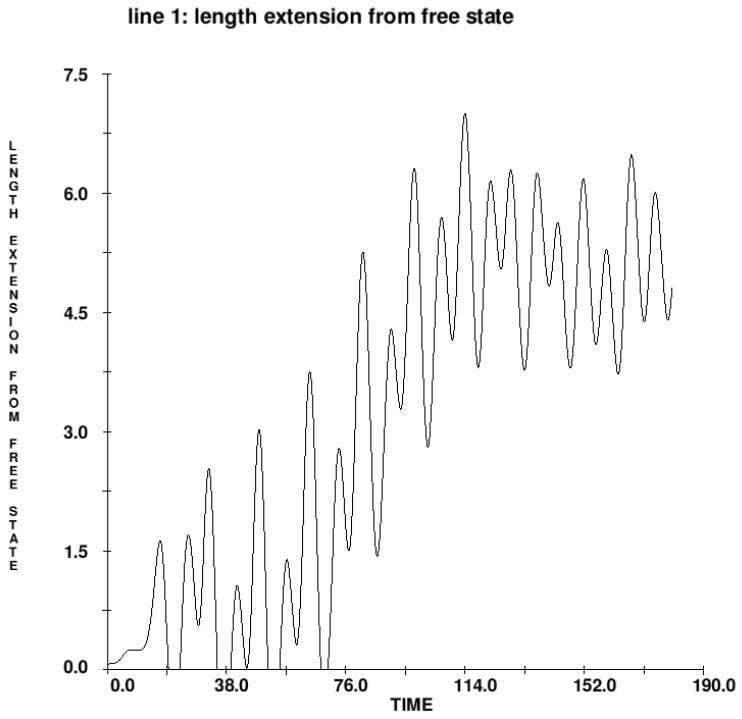

(a)

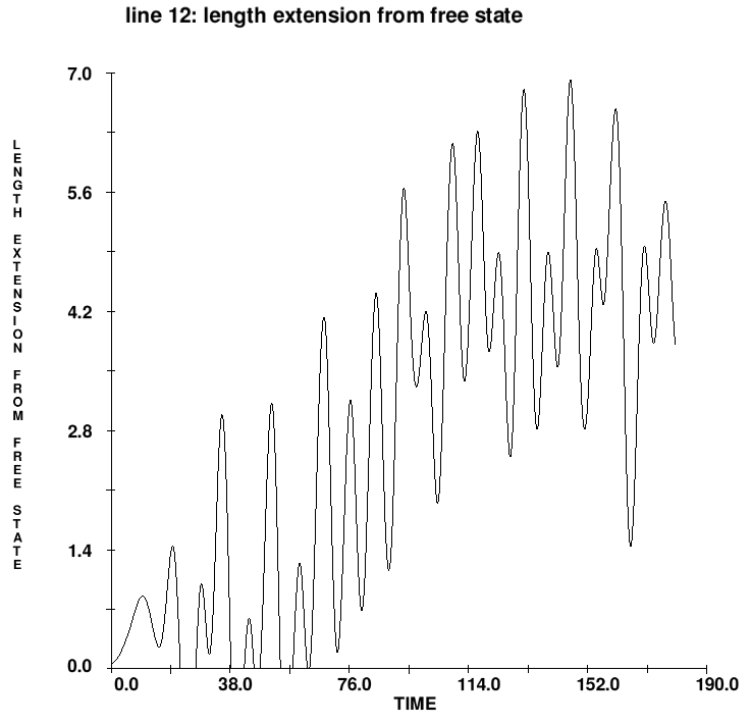

(b)

Figure 9. Extension (in m) versus time (in s) for mooring lines at front (a) and back (b) of platform,

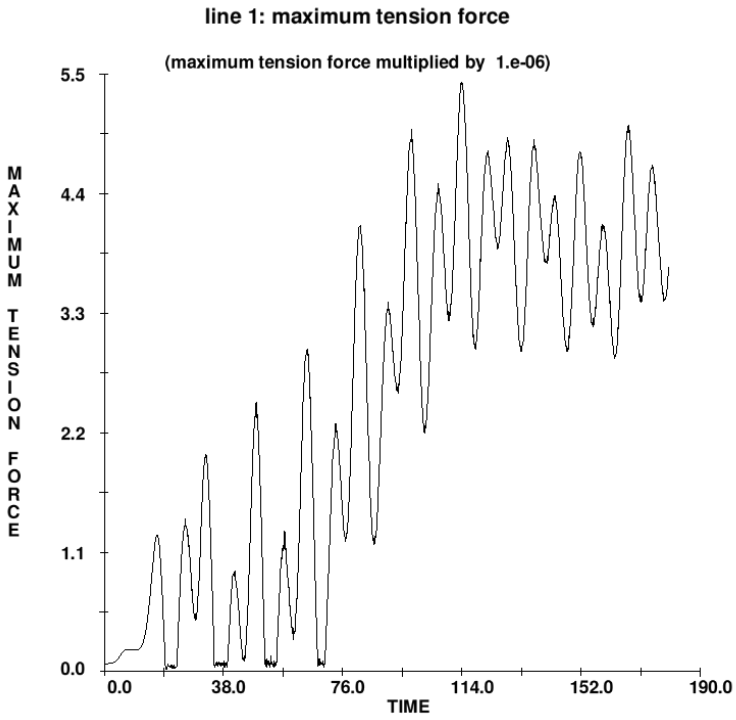

(a)

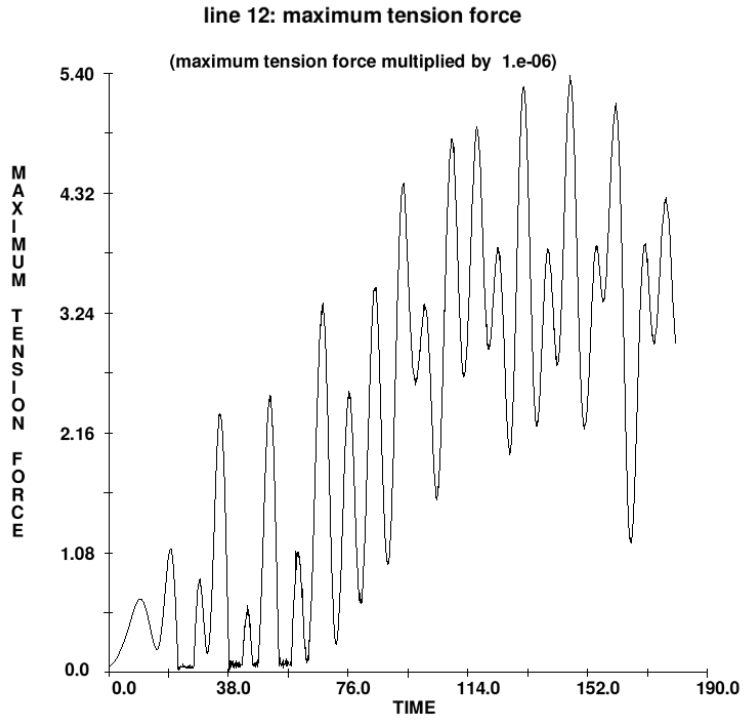

(b)

Figure 10. Maximum tension (in N) versus time (in s) for the mooring lines at the front (a) and back (b) of the platform.

5. Conclusions

A compliant mooring line model has been developed and implemented in ***FLOW-3D***® version 11.1. Multiple mooring lines with different length, diameter, mass density and spring coefficients are allowed. Each mooring line can have both of its ends connected to moving objects or one end connected to a moving object and the other anchored at a fixed location. The mooring lines can be taut or slack and may fully or partially rest on the sea/river bed. They can be porous and permeable to water but flow inside mooring lines is not calculated. The model uses a finite segment approach to calculate the full 3D dynamics of mooring lines and the dynamic coupling between mooring lines and moving objects. Gravity, buoyancy, fluid drag and tension are all considered for mooring lines. Instantaneous mooring line shape, extension and tension distribution are calculated. Static equilibrium is assumed for the initial condition of each mooring line.

When a mooring line is anchored deep in the water, its lower part can be located outside the domain. In such case, a uniform water velocity, or current, is assumed below the domain, and the drag force is evaluated using that velocity for that part of the line.

The model was validated for a catenary mooring line in static equilibrium. Close match between the computed and analytical results were obtained. The model was also applied to a moored floating platform in open sea. The result was reasonable, and the model's capability to simulate complex mooring systems was successfully demonstrated.

The mooring line model has limitations. It does not consider the bending stiffness of the mooring lines. Interactions between mooring lines are also ignored. When simulating mooring line networks, free nodes are not allowed. Collisions with solid objects are also not considered, thus the lines may penetrate solid objects after coming in contact.

References

Dean, R. and Dalrymple, R., 1991, *Water Wave Mechanics for Engineers and Scientists*, World Scientific.

DuBuque, G. 2011, *A Lumped Parameter Equilibrium Model of a Submerged Body with Mooring Lines*, Master thesis, University of Washington.

Irvin, M., 1981, *Cable Structures*, Dover Publications Inc., New York.

Nichol, T., 2014, *Numerical Modeling of Compliant-Moored System Dynamics with Applications to Marine Energy Converters*, Master thesis, University of Washington.

Raman-Nair, W. and Baddour R. E., 2002, *Three-dimensional coupled dynamics of a buoy and multiple mooring lines: Formulation and algorithm*, The Quarterly Journal of Mechanics & Applied Mathematics, **55**(2), 179–207.